Physicochem. Probl. Miner. Process., 62(1), 2026, 216390

http://www.journalssystem.com/ppmp

Physicochemical Problems of Mineral Processing

ISSN 1643-1049

Improving flotation recovery of gold in a refractory gold ore: An integrated approach between response surface methodology and automated quantitative mineralogy

Abdelkhalek Barbouchi [1,2], Kaoutar Dachri [2], Tariq Labbilta [2], Khalid Naji [2], Hakim Faqir [2], Intissar Benzakour [2], Rachid Idouhli [1], Mohy-eddine Khadiri [1], Abdessalem Abouelfida [1], Jaouad Benzakour [1]

[1] Laboratory of Physicochemistry of Materials and Environment, Department of Chemistry, Faculty of Science Semlalia, Cadi Ayyad University, BP 2390, Marrakech, Morocco

[2] Reminex Research Center, Managem Group, BP 469, 40000 Marrakech, Morocco

Corresponding author: a.barbouchi.ced@uca.ac.ma (Abdelkhalek Barbouchi)

Abstract: For the pretreatment of refractory sulfidic gold ores, processing gold-rich concentrates instead of ore offers several advantages, mainly enhancing cost-effectiveness of the process. In this study, an integrated approach combining experimental design and automated quantitative mineralogy (AQM) was developed to optimize gold flotation recovery from a refractory gold ore. Complete ore characterization using AQM and scanning electron microscopy (SEM) revealed that gold occurs as nanoscale inclusions (288.8–489.5 nm) within pyrite and arsenopyrite. Mineral mapping showed a composition dominated by silicates and minor sulfides. Optimal flotation conditions were determined using a Doehlert design, with pH and particle size distribution (D80) as variables. The optimized conditions (pH = 9.56, D80 = 88 µm) yielded a gold recovery of 86.76% and a concentrate gold grade of 18.80 ppm, compared to 2.61 ppm in the feed. Modal mineralogy and particle mapping indicated that the concentrate was enriched in sulfides (pyrite 58.9%, arsenopyrite 6.6%), while the tailing was mainly silicates (quartz 34.6%, albite 26.2%, muscovite 18%), confirming effective sulfide-gangue separation. Gold remaining in the tailing was enclosed in albite and quartz, demonstrating that the achieved recovery is ultimate, as this gold is non-floatable. The enhanced recovery and grade at higher pH were attributed to the improved stability of potassium amyl xanthate under alkaline conditions, as confirmed by Fourier Transform Infrared (FTIR) spectroscopy.

Keywords: refractory gold ore, gold flotation, mineral liberation, automated quantitative mineralogy, doehlert design, process optimization

1. Introduction

With the depletion of free-milling gold resources in the last decades, the gold mining industry has shifted its attention to the extraction of gold from refractory ores. These materials are distinguished by their low gold recovery rates using conventional cyanidation methods (Barbouchi et al., 2025a, Rogozhnikov et al., 2021). Typically, the gold ores are defined as refractory when the yield of gold extraction is less than 80% (Mesa Espitia and Lapidus, 2015; Rodríguez-Rodríguez et al., 2018). In sulfidic refractory gold ores, fine gold particles are often finely disseminated and encapsulated within sulfide minerals such as pyrite and arsenopyrite (Barbouchi et al., 2024a, 2024b). Therefore, the ore must be processed using an appropriate pretreatment method, such as roasting, bacterial oxidation, or pressure oxidation (Barbouchi et al., 2024c; Hammerschmidt et al., 2016; Miller and Brown, 2016; Thomas and Pearson, 2016).

Depending on the ore's mineralogy and gold content, it is generally preferable to process gold-rich concentrates rather than the ore itself. This is achieved by producing sulfide concentrates through beneficiation techniques such as flotation (Badri and Zamankhan, 2013). The resulting gold

DOI: 10.37190/ppmp/216390

concentrate typically contains substantial amounts of gold and sulfide minerals (e.g pyrite and arsenopyrite) which are the primary carriers of gold. Processing gold-rich concentrates instead of the whole ore has a number of advantages, not least of which is the improved cost-effectiveness of the pretreatment process (Barbouchi et al., 2024c). In addition, a high sulfide content in the concentrate is a critical factor for the efficiency of pretreatment methods such as roasting and bio-oxidation. In roasting, the exothermic behavior of sulfide oxidation reduces fuel requirements and thus energy consumption (Lunt and Weeks, 2016). On the other hand, for the bio-oxidation pretreatment, a high sulfide content promotes bacterial activity, as sulfides create a favorable environment for the living and growth of acidophilic bacteria (Jia et al., 2019).

Flotation of refractory sulfidic gold ore is an efficient process used to concentrate gold by selectively separating gold and gold-bearing minerals from the gangue materials. The hydrophobicity of gold is increased by the addition of flotation collectors, such as xanthates, which are commonly used in sulfide mineral flotation (Chryssoulis and Dimov, 2004). Potassium Amyl Xanthate (PAX) is the most widely used collector for the flotation of native gold and gold-bearing minerals (Allan and Woodcock, 2001). According to a 2012 industrial survey, out of 12 flotation plants processing gold-bearing iron sulfides, 11 of them use PAX as principal collector (Dunne, 2016).

The optimal flotation conditions for recovering gold are primarily influenced by several mineralogical factors as gold typically exists in multiple forms within the ore. This includes the mineralogy of both the gold-bearing and gangue minerals, mineral associations and locking, the liberation profile of the gold-bearing minerals and the particle size of the gold itself (Zhou and Gu, 2016). Automated quantitative mineralogy (AQM) analysis is a powerful tool for acquiring this information. It relies on advanced analytical techniques such as scanning electron microscopy (SEM) combined with energy dispersive spectroscopy (EDS) and sophisticated software for precise mineralogical quantification (Zhou and Gu, 2016).

The pH of the pulp significantly influences the flotation performance of gold and gold-bearing sulfides, by affecting surface charge and collector adsorption, and is commonly controlled using lime or sulfuric acid as pH modifiers (Dunne, 2016). According to (Allan and Woodcock, 2001), pyrite and its encapsulated gold exhibit optimal flotation performance under both acidic (pH 4) and alkaline (pH 8) conditions, allowing efficient flotation recovery. Also, arsenopyrite, exhibiting similar properties to pyrite, has flotation conditions closely aligned with those of pyrite. However, these observations have been demonstrated primarily at the laboratory scale. In industrial gold flotation circuits, operations are generally conducted under near neutral to alkaline conditions to ensure safer reagent handling and to minimize equipment corrosion (Dunne, 2016).

Recent advances in flotation theory have greatly improved the understanding of the complex physicochemical phenomena governing the recovery of gold and gold-bearing sulfides. Beyond classical concepts of adsorption, surface oxidation, and wettability, contemporary research highlights the critical roles of electrochemical reactions, mineral surface charging, hydrodynamic–chemical coupling, and the formation of intermediate species such as dixanthogen during the flotation process (Feng et al., 2025; Mikali et al., 2023; Moslemi and Gharabaghi, 2017; Tang et al., 2026; Yang et al., 2025).

The flotation process can be optimized using several models, such as orthogonal designs and response surface designs. Orthogonal models are mainly used for factor screening and provide limited information on curvature, making them insufficient for modeling complex responses (Xue et al., 2026). Response surface designs such as Box-Behnken and Central Composite Design (CCD) improve on this by allowing quadratic modeling, but they have their own limitations. CCD requires factorial and axial points that often exceed practical or safe experimental ranges (Bu et al., 2016), while Box-Behnken places points in the middle of the domain, leaving some regions of the experimental space unexplored (Gao et al., 2022; Ren et al., 2024; Zhou et al., 2023). In contrast, the Doehlert design distributes experimental points uniformly across the entire experimental domain, offering high rotatability and consistent prediction accuracy. It also allows each factor to be studied at a different number of levels, providing greater flexibility and reducing the total number of experiments required (Brown, Tauler, & Walczak, 2009; Cerqueira et al., 2021). These characteristics make Doehlert's design particularly effective and suitable for optimizing the flotation process, where comprehensive exploration of the experimental domain and reliable response modeling are essential for successful optimization.

The aim of this paper is to improve and optimize the flotation recovery of gold in a refractory sulfidic gold ore using an integrated approach between experimental design and AQM. The effect of pH and particle size distribution (D80) was examined using the Doehlert design in combination with response surface methodology (RSM). The use of these statistical tools allowed for minimizing the number of experiments and evaluating the relative impact of experimental factors, as well as their interactions. Also, a comprehensive mineralogical investigation was conducted to provide insights into modal mineralogy, liberation, association, and locking of gold and gold-bearing minerals in the flotation process streams.

2. Materials and methods

2.1. Ore sample

The refractory gold ore used in this study was obtained from the Tri-K gold mine (Managem Group), located in the Mandiana region, Republic of Guinea. The ore sample was crushed using a jaw crusher, and then ground by a laboratory ball mill. The particle size distribution (D_{80}) of the ground ore was determined using a series of standard sieves in a vibrating sieve shaker. After sieving, the material retained on each sieve was dried and weighed, and the cumulative mass distribution was used to calculate the D_{80}. The procedure followed the ASTM C136 standard. The ground ore adjusted to the target D_{80} was then used as the feed for the flotation tests.

2.2. Flotation procedure

The flotation tests were carried out on 1000 g of mill ore (solids concentration of 67%). The product was fed to a 3-liter flotation cell, and the slurry was adjusted to 33% solids. All flotation experiments were carried out using a Metso laboratory machine. The flotation time was 15 min divided into 3 roughers (Fig. **1**). The speed of impeller was fixed at 1200 rpm, and the air flow rate was fixed to 6 L/min. The pH was adjusted using lime (20%) and sulfuric acid (20%). Potassium Amyl Xanthate (PAX) and Methyl IsoButyl Carbanol (MIBC) were used respectively as collector and frother. The conditions of flotation experiments are given in Table 1.

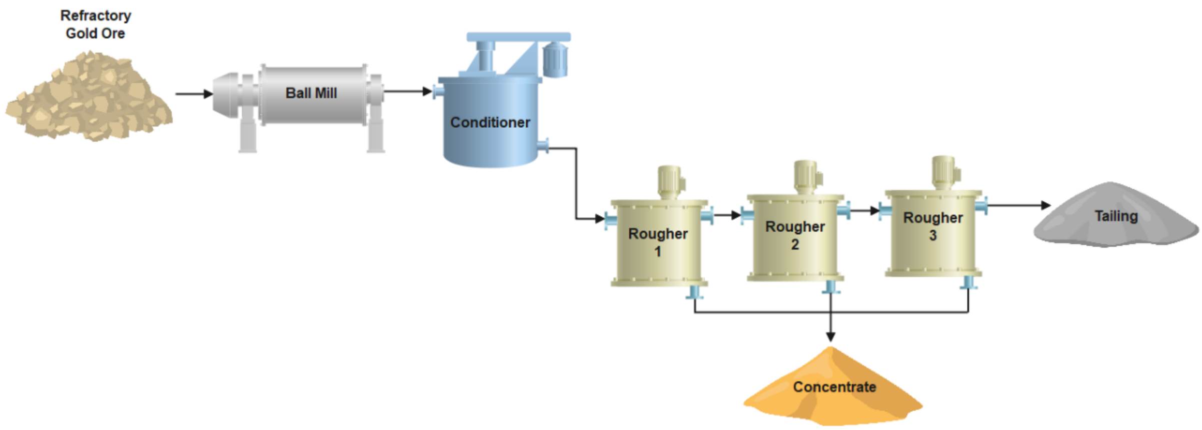

Fig. 1. Flotation flowsheet

After flotation experiments, the slurry was filtered and the gold concentrates and tailing were dried, weighed and analyzed for gold content. The final products were combined to form one cumulative concentrate allowing the calculation of the global gold recovery using equation (**1**).

$$GR = \frac{m_c \times G_c}{m_f \times G_f} \times 100 \quad (1)$$

where GR is gold recovery, m_c and m_f are the weights of the concentrate sample and the feed samples respectively, G_c and G_f are the elemental grade of gold in the concentrate and feed samples respectively.

Table 1. Description of flotation conditions

Milling conditions	
Media	Stainless steel
Mill volume	10 L
% Solids	67%
Description of pulp	
Mass of solids	1 kg
Size distribution, D_{80}	[40 µm, 100µm]
% Solids	33%
pH	[6 – 10]
Flotation cell settings	
Flotation time	15 min
Air flow rate	6 L/min
Impeller speed	1200 rpm
Flotation reagents	
PAX	60 g/t
MIBC	10 g/t
Lime (20%) / Sulfuric acid (20%)	pH regulators

2.3. Chemical analysis

The gold content in the ore, flotation concentrate and flotation tailing was analyzed by fire assay method followed by atomic absorption spectroscopy (AAS) using Agilent 280 FS Flame machine. The content of iron (Fe) and arsenic (As) in the ore was analyzed by AAS after acid digestion. The contents of other elements were analyzed by inductively coupled plasma-optical emission spectrometer (ICP-OES) using Agilent 5110 SVDV machine. FTIR spectroscopy was used to identify functional groups with their corresponding vibration modes of the studied collector at different pH. The analysis was performed with a VERTEX 70 FT-IR Spectrometer, equipped with an attenuated total reflection (ATR) accessory.

2.4. Mineralogical characterization

The mineralogical characterizations of the refractory gold samples (feed, flotation concentrate and flotation tailing) were conducted through AQM. This analysis was carried out with a Carl Zeiss Sigma VP microscope fitted with two Bruker X-Flash 6130 EDS detectors. The resulting mineralogical data were then processed using the Mineralogic software and reported on the Mineralogic Reporter platform. All characterizations were performed at 20 kV using a Backscattered Electron detector and a diaphragm aperture set to 120 µm. The samples were prepared into polished thin sections. For the ore sample, the mineralogical characterization was additionally conducted using scanning electron microscopy (SEM) in order to determine the mesh size of gold particles.

2.5. Experimental design

The optimization of gold flotation in the studied refractory gold ore was conducted using Doehlert's experimental design. This method is highly effective for assessing the significance of each studied factor and determining the optimum levels at which these factors should be maintained to maximize process performance (Barbouchi et al., 2025b) . In addition, it allows the response to be represented across the entire experimental domain of factors with minimal number of experiments, enabling the response to be predicted at any point in the domain (El Maguana et al., 2018). In this study, the examined factors are pH and particle size distribution (D_{80}) (Table 2).

The matrix of Doehlert experimental design and the corresponding experimental conditions are presented in Table 3. The center of the experimental domain was repeated three times to assess experimental error and response reproducibility.

Table 2. Experimental domains for the Doehlert's experimental design

Factors	Undimensional variables	Experimental domain
U_1: D_{80} (µm)	X_1	40 to 100
U_2: pH	X_2	6 to 10

Table 3. Doehlert experimental design matrix and experimental conditions

N° Exp.	Doehlert's experimental design		Experimental conditions	
	X_1	X_2	U_1 µm	U_2
1	1.00000	0.00000	100	8.00
2	-1.00000	0.00000	40	8.00
3	0.50000	0.86603	85	9.73
4	-0.50000	-0.86603	55	6.27
5	0.50000	-0.86603	85	6.27
6	-0.50000	0.86603	55	9.73
7	0.00000	0.00000	70	8.00
8	0.00000	0.00000	70	8.00
9	0.00000	0.00000	70	8.00

The analyzed responses are the yield of gold recovery (GR) and the gold grade (GG) in the flotation concentrate, which are correlated with pH and D_{80} factors using the polynomial model as represented by equation (**2**).

$$GR\ /\ GG = b_o + \sum_{i=1}^{2} b_i X_i + \sum_{i=1}^{2} b_{ii} X_{ii}^2 + \sum_{1 \le i \le j \le 2}^{2} b_{ij} X_i X_j \quad (2)$$

where X_1 and X_2 are the coded variables of pH and D_{80} respectively. b_0 is a constant, while b_1, b_2 are represent the weights of pH and D_{80} respectively. b_{12} represents the interaction effect between pH and D_{80}. The validity of the model was assessed using the ANOVA results. Nemrodw software was used to design the statistical experiments, estimate the coefficients and analyze the results.

3. Results and discussion

3.1. Sample characterization

3.1.1. Chemical analysis

The average assay of three samples from the studied ore showed a gold grade of 2.61 g/t. Chemical analysis revealed the presence of 4.25% iron, 0.24% arsenic and 0.83% sulfur and 59.57% SiO_2 (Table 4).

Table 4. Chemical composition of the ore

Element	Au (ppm)	Fe	As	S	SiO_2	Al_2O_3	CaO	MgO
Content, %	2.61	4.25	0.24	0.83	59.57	11.81	2.46	2.81

3.1.2. Granulochemical analysis

The results of the granulochemical analysis of the gold ore sample (Fig**. 2**) identified higher contents of Au, Fe, S and As in the finer fractions (-20 µm), with a proportion of 51.91%, 57.62%, 44.58% and 57.11% respectively. The analysis revealed also a slightly higher contents of these elements in the fractions (+20, +40 µm and +63 µm). These results show that gold and its mineral hosts (pyrite and arsenopyrite) are mainly very fine-grained.

3.1.3. SEM characterization

SEM results (Fig. **3**) confirm the fine size of gold particles observed in the granulochemical analysis. Gold particles were identified at the nanoscale as inclusions within pyrite and arsenopyrite, with sizes ranging from 288.8 nm to 489.5 nm. These findings suggest that effective recovery of pyrite and arsenopyrite is critical during the flotation process to maximize the gold recovery.

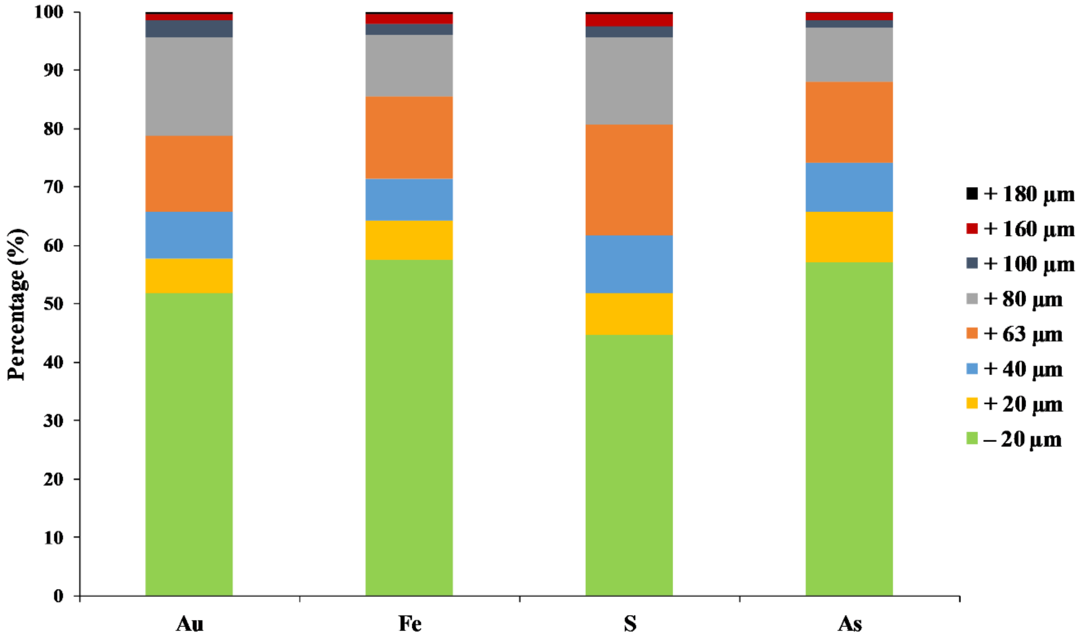

Fig. 2. Granulochemical analysis of Au, Fe, S and As in the ore sample

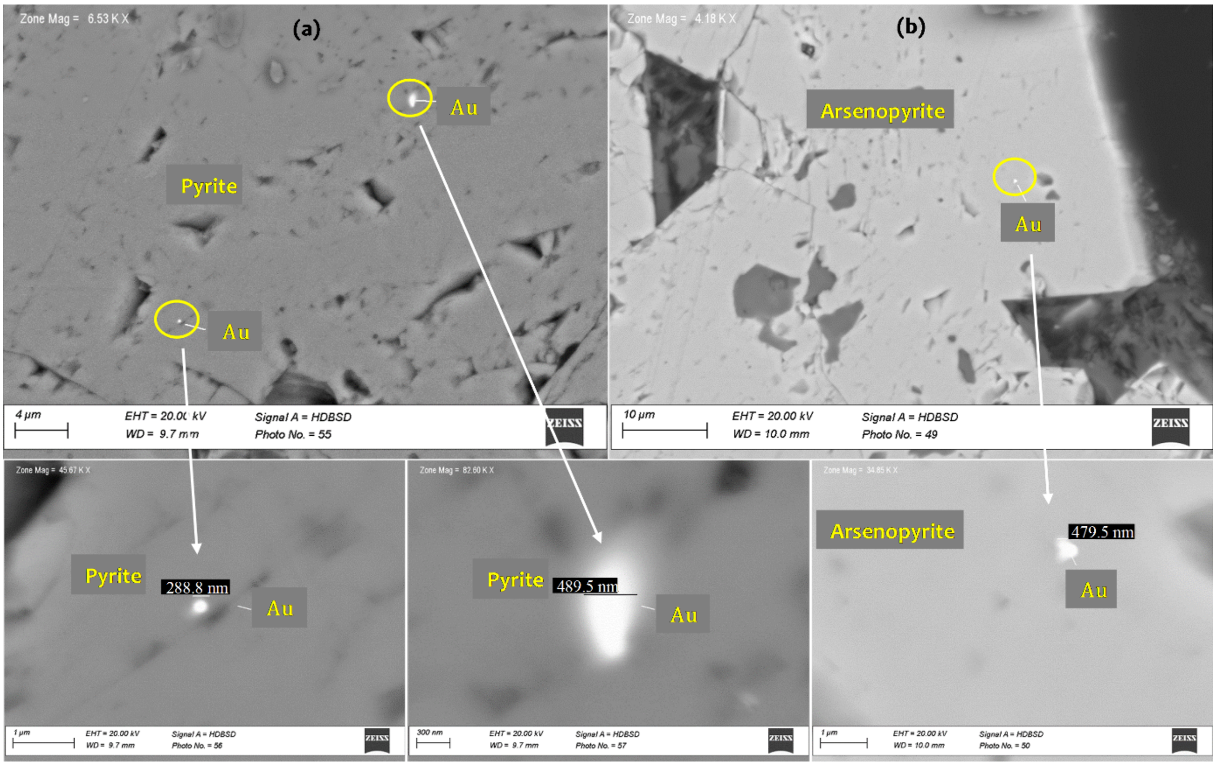

Fig. 3. SEM images of polished section of the crushed sample showing gold mineral associations

3.2.4. Modal mineralogy

Mineral mapping and the modal mineralogy of the feed sample showed a mineral gangue composed mainly of silicate minerals (Fig. 4), with albite (36%), quartz (33.1%) and clay minerals (13.2%) as primary components. In addition, iron oxide is present in the gangue with an abundance of 6%. Sulfide minerals represented by pyrite and arsenopyrite have abundances of 2.1% and 0.3% respectively. Gold is present in trace amounts, at less than 0.1%.

(a)

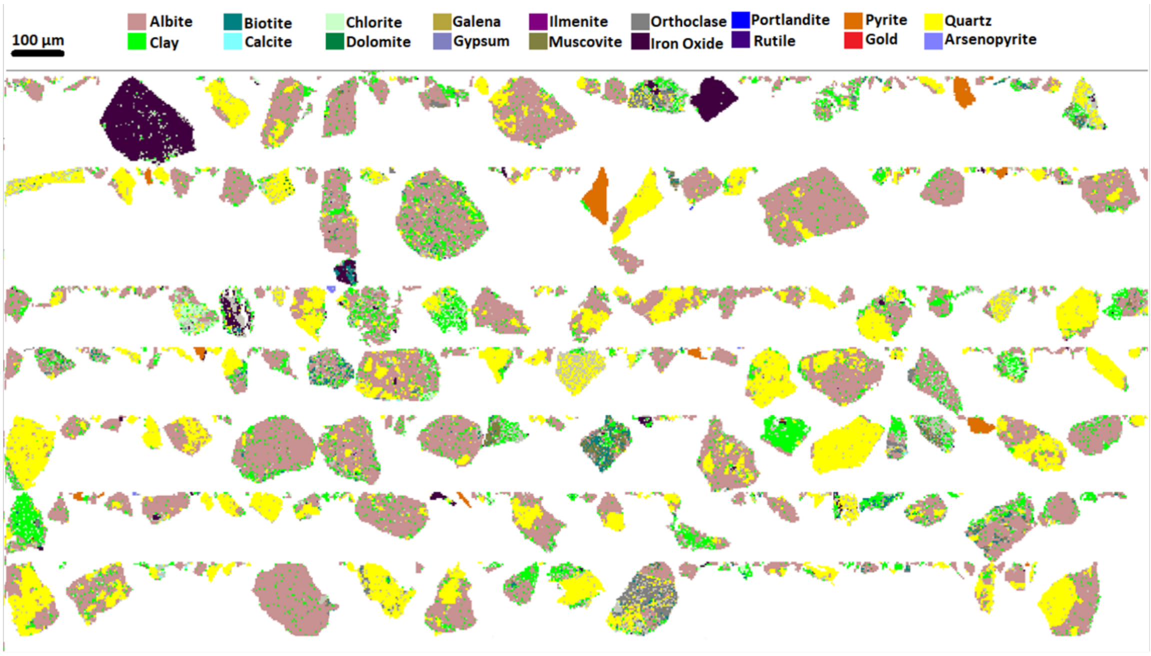

(b)

Mineral phases	Chemical formula	Mineral abundance (%) Feed
Gold	Au	<0.1
Pyrite	FeS_2	2.1
Arsenopyrite	FeAsS	0.3
Quartz	SiO_2	33.1
Albite	$NaAlSi_3O_8$	36.0
Muscovite	$KAl_2(Si_3Al)O_{10}(OH)_2$	2.8
Clay	$Al_2O_3.\ 2SiO_2.\ 2H_2O$	13.2
Biotite	$K(Mg.Fe)_3AlSi_3O_{10}(F.OH)_2$	2.3
Orthoclase	$KAlSi_3O_8$	1.7
Chlorite	$(Mg.Fe)\ _3(Si.Al)\ _4O\ _{10}(OH)\ _2$	2.3
Iron oxide	$Fe_2O_3.\ Fe_3O_4$	6.0
Calcite	$CaCO_3$	<0.1
Dolomite	$CaMg(CO3)_2$	<0.1
Rutile	TiO_2	0.1
Gypsum	$CaSO\ _4{\cdot}2H_2O$	<0.1
Portlandite	$Ca(OH)_2$	<0.1
Ilmenite	$(FeTi)2O_3$	<0.1
Galena	PbS	<0.1

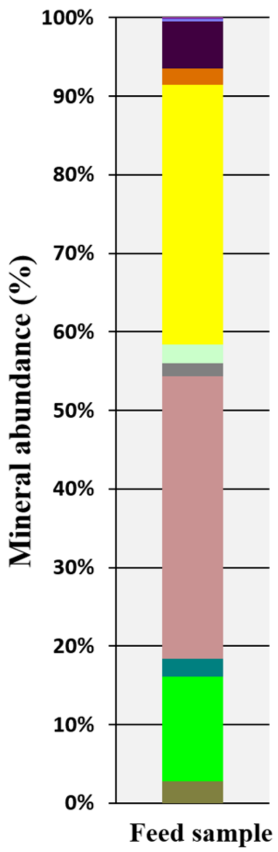

Fig. 4. Particle mapping (a) and mineral abundance (b) of feed sample

3.2.5. Liberation, association, and locking

The liberation analysis of the target minerals showed that pyrite and arsenopyrite grains are predominantly liberated (free surface > 80%), with liberation rates of 83% and 78%, respectively. The middling fraction (20% < free surface < 80%) represented a range of 5% for the pyrite and 8% for the arsenopyrite (Fig. 5.a). According to the association diagrams (Fig. 5.b), pyrite grains are primarily associated with clay minerals (26%), chlorite (20%) and iron oxide (13%), while arsenopyrite is mostly associated to the pyrite with a percentage of 35%. Locked particles (free surface < 20%) of pyrite are principally encased in clay minerals (23%), iron oxides (17%) and albite (6%). For arsenopyrite, locked grains are enclosed in pyrite (51%), clay minerals (10%) and iron oxide (7%) (Fig. 5.c). All of the gold grains are locked (Fig. 5.a), they are primarily encapsulated into pyrite showing a percentage of 35% (Fig. 5.c) and arsenopyrite (19%).

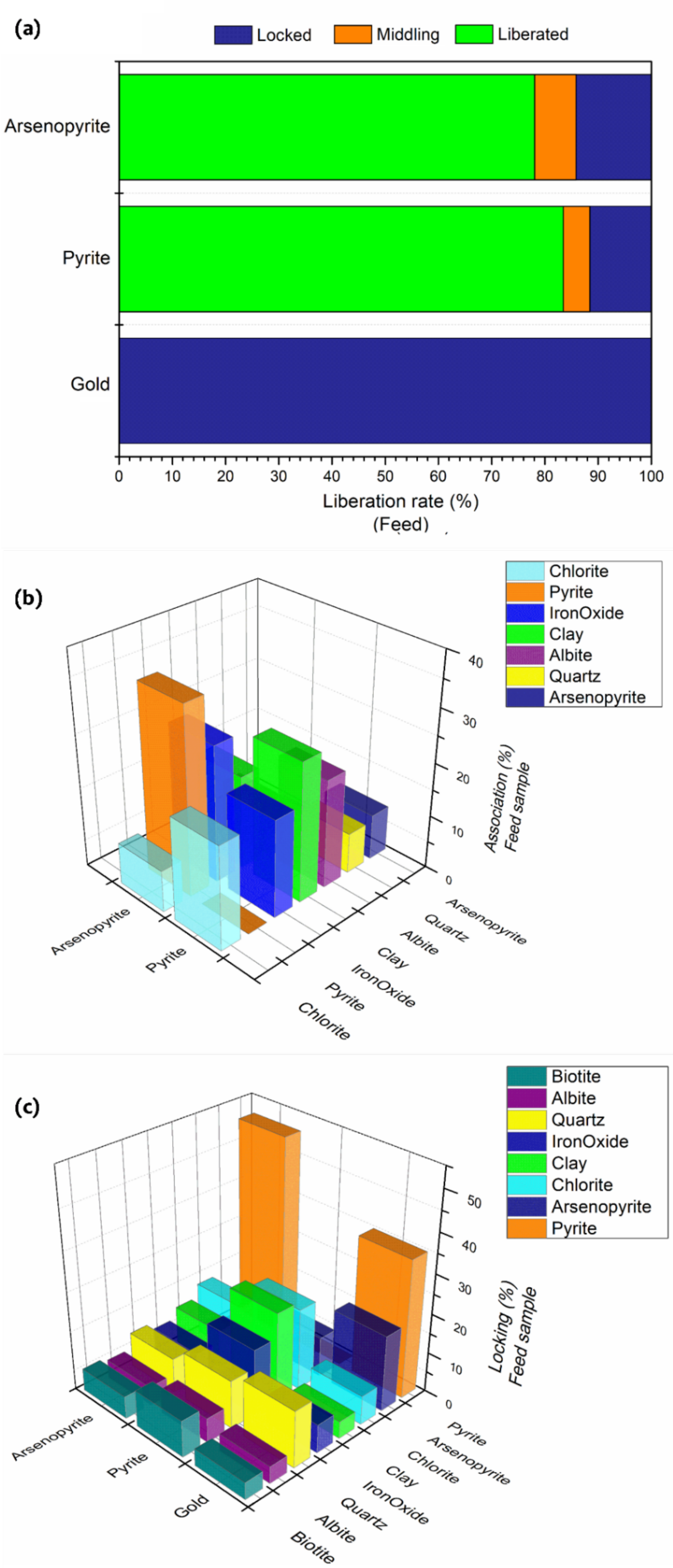

Fig. 5. Liberation (a) association (b) and locking (c) data of target minerals in feed sample

3.2. Effect of flotation factors on gold recovery and gold grade

The analysis of the experimental results, as summarized in Table 5, indicates that the yield of gold recovery (GR) and the assay of gold grade (GG) vary from 73.81% to 89.39% and from 7.18 ppm to 23.16 ppm respectively.

The estimated values of the coefficients are shown in Table 6. The analysis of the various factors shows that both the gold recovery and the gold grade are slightly negatively influenced by D_{80} (b_1 = -1.628 and b_1 = -2.292 respectively), whereas they are positively affected by pH (b_2 = 7.254 and b_2 = 7.451 respectively). pH is the most significant factor. Additionally, the interaction observed between D_{80} and pH is slightly significant for the gold recovery (b_{12} = 0.375) compared to the gold grade (b_{12} = 0.260).

Table 5. Experimental conditions and experimental results

N° Exp.	Experimental conditions		Experimental responses	
	U_1	U_2	GR	GG
	μm		(%)	(ppm)
1	100	8.00	83.20	14.50
2	40	8.00	85.07	18.30
3	85	9.73	86.70	20.31
4	55	6.27	77.15	10.48
5	85	6.27	73.81	7.18
6	55	9.73	89.39	23.16
7	70	8.00	84.23	13.44
8	70	8.00	83.57	14.07
9	70	8.00	85.11	12.84

Table 6. Estimated values of coefficients for the gold recovery and gold grade responses

Coefficient	GR		GG	
		Significance (%)		Significance (%)
b_0	84.303	< 0.01 ***	13.450	< 0.01 ***
b_1	-1.628	9.4	-2.292	1.30 *
b_2	7.254	0.171 **	7.451	0.0424 ***
b_{11}	-0.168	88.4	2.950	2.28 *
b_{22}	-3.332	5.2	1.460	12.2
b_{12}	0.375	79.9	0.260	78.3

*** Statistically significant at the level < 99.99%

** Statistically significant at the level 99%

* Statistically significant at the level 95%

The yield of gold recovery (equation 3) and the gold grade (Eq. 4) can be expressed as follows:

$$GR=84.303-1.628X_1+7.254X_2-0.1682X_1^2-3.332X_2^2-0.375X_1X_2 \quad (3)$$

$$GG=84.303-1.628X_1+7.254X_2-0.1682X_1^2-3.332X_2^2-0.375X_1X_2 \quad (4)$$

The ANOVA results (Table 7) indicate that the proposed models (Eqs. 3–4) effectively describe the variation in gold recovery (GR) and gold grade (GG) as functions of the studied experimental factors. The regression for GR (F = 26.42, $p < 0.05$) and GG (F = 69.31, $p < 0.05$) is significant, while the lack-of-fit tests are non-significant (GR: F = 4.83, p = 0.159; GG: F = 2.43, p = 0.259), confirming that the models adequately fit the experimental data. Moreover, the high adjusted R^2 values (94.1% for GR and 97.7% for GG) demonstrate that the polynomial models accurately explain the majority of observed responses, validating their reliability.

Table 7. ANOVA results and adjusted root-square values associated to the adopted polynomials models

	Source of variation	Sum square	Degree of freedom	Mean square	F-ratio	Signif.	R^2_{Adj}	Lack-of-Fit F	Lack-of-Fit p-value
GR (%)	Regression	179.5693	5	35.9139	26.4193	1.10 *	0.941	4.83	0.159
	Residues	4.0781	3	1.3594					
GG (ppm)	Regression	193.7340	5	38.7468	69.3138	0.268 **	0.977	2.43	0.259
	Residues	1.6770	3	0.5590					

The response surfaces, presented as two- and three-dimensional plots in Fig. 6, indicate that increasing the pH of the slurry improves both the gold recovery and the gold grade in the concentrate, whereas reducing D_{80} enhances slightly them. The analysis further reveals that optimal gold recovery and gold grade are achieved at pH above 8 and D_{80} above 70 µm. These findings are in agreement with the granulochemical (Fig. 2) and SEM (Fig. 3) analyses, which revealed that gold and its mineral hosts are predominantly fine-grained. Consequently, D_{80} has a slightly impact, as even extensive milling is insufficient to fully liberate gold for effective recovery via flotation.

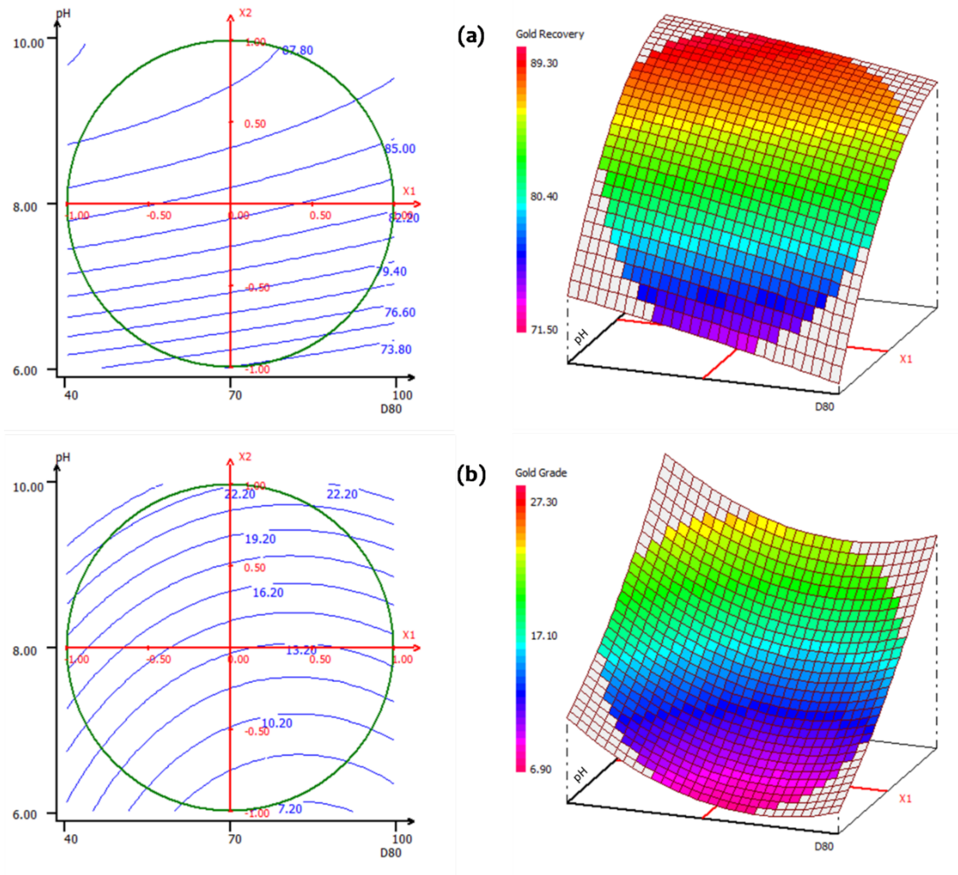

Fig. 6. Two- and tri-dimensional representations of the variation of gold recovery (a) and gold grade (b) as function of the studied factors

3.3. Optimization of gold flotation conditions

To identify the optimum flotation conditions of gold for achieving both high gold recovery and high gold grade, the desirability function was used to simultaneously optimize experimental factors. The desirability function ranges from 0 to 1, where a value of 0 indicates an unsatisfactory response and a value of 1 represents the desired value. The maximum value of the desirability function represents the best compromise for the two responses (GR and GG) within the experimental domains of the studied factors, and predicts the optimal experimental conditions (El Maguana et al., 2018). The results of the multicriteria optimization are given in Table 8. The optimum conditions corresponding to the maximum overall desirability function are identified as pH = 9.56 and D_{80} = 88 µm. Under these conditions, the predicted gold recovery and gold grade calculated from the model are 87.19% and 19.21 ppm respectively. To validate these predicted values, three flotation tests were carried out under the aforementioned optimum conditions. The average experimental responses obtained from the three flotation tests are 86.76 % ± 1.73 for the gold recovery and 18.80 ppm ± 0.49 for the gold grade. The minimal difference between experimental and predicted values validates the high accuracy of the model.

Table 8. Characteristics of maximum for responses: gold recovery and gold grade

Response	Cal. value	Weight	d_i %	$d_{i\,min}$ %	$d_{i\,max}$ %	Exp. value
Gold recovery (%)	87.19	1	100.00	100.00	100.00	86.76 ± 1.73
Gold grade (ppm)	19.21	1	100.00	100.00	100.00	18.80 ± 0.49
Desirability			100.00	100.00	100.00	

d_i: partial desirability of response Y_i, $d_{i\,min}$: minimal partial desirability of response $Y_{i,\,di\,max}$: maximal partial desirability of response Y_i, Cal. value: calculated value and Exp. value: experimental value

The flotation results under optimized conditions (**Table 9**) demonstrate that 61.72% of the gold was recovered in the initial stage, with a grade of 24.62 ppm from a feed of 2.57 ppm, suggesting rapid gold flotation kinetics. The overall gold recovery was 86.93%, with a final tailing of 0.39 ppm. This recovery correlates with that of sulfur, due to the presence of gold dispersed in pyrite and arsenopyrite. The global recovery of sulfur was 76.28%. The flotation results showed also good separation of the sulfides from the gangue, with only 12.45% of SiO_2 floated, demonstrating good selectivity of the flotation process for the studied ore.

Table 9. Flotation results under optimized conditions

	Weight		Grade			Recovery (%)		
	(g)	(%)	Au (ppm)	S (%)	SiO_2 (%)	Au	S	SiO_2
Rougher 1	65.8	6.4	24.62	8.35	53.87	61.72	53.56	5.27
Rougher 2	45.3	4.4	12.17	3.88	62.47	21.00	17.13	4.21
Rougher 3	30.2	3.0	3.66	1.90	66.36	4.21	5.59	2.98
Tailing	879.5	86.2	0.39	0.28	66.98	13.07	23.72	87,55
Feed (calculated)	1020.8	100	2.57	1.00	65.92	100	100	100
Feed (direct)			2.61	0.83	66.57			
Recovery (%)		**13.84**				**86.93**	**76.28**	**12.45**

3.4. Discussion

As revealed from the experimental design, the optimal flotation conditions of gold for the studied refractory gold ore are pH = 9.56 and D_{80} = 88 µm. The concentrate and tailing obtained under these conditions are characterized by automated quantitative mineralogy. The modal mineralogy of the concentrate and tailings samples is shown in Fig. **7**. The mineralogical composition of the concentrate sample is dominated by sulfide minerals, represented respectively by pyrite (58.9%) and arsenopyrite (6.6%). Conversely, the tailing sample is mainly composed of silicates represented by quartz (34.6%), albite (26.2%) and muscovite (18%). These findings highlight the effective separation between the target sulfides and the gangue during the flotation of the studied ore, further validating the optimal conditions determined by the experimental design.

In addition, the particle mapping confirmed the modal mineralogical findings for both concentrate and tailing samples according to Fig. 8. In the concentrate, pyrite grains dominate, with a small

Mineral phases	Chemical formula	Mineral abundance (%)	
		Concentrate	Tailing
Gold	Au	<0.1	<0.1
Pyrite	FeS_2	58.9	<0.1
Arsenopyrite	FeAsS	6.6	<0.1
Quartz	SiO_2	4.9	34.6
Albite	$NaAlSi_3O_8$	11.5	26.2
Muscovite	$KAl_2(Si_3Al)O_{10}(OH)_2$	0.6	18.0
Clay	Al_2O_3. $2SiO_2$. $2H_2O$	11.1	7.9
Biotite	$K(Mg,Fe)_3AlSi_3O_{10}(F,OH)_2$	1.0	5.5
Orthoclase	$KAlSi_3O_8$	0.3	3.7
Chlorite	$(Mg,Fe)_3(Si,Al)_4O_{10}(OH)_2$	2.3	2.1
Iron oxide	Fe_2O_3. Fe_3O_4	2.5	1.8
Calcite	$CaCO_3$	0.1	<0.1
Dolomite	$CaMg(CO3)_2$	<0.1	<0.1
Rutile	TiO_2	<0.1	<0.1
Gypsum	$CaSO_4 \cdot 2H_2O$	<0.1	<0.1
Ilmenite	$(FeTi)2O_3$	<0.1	<0.1
Galena	PbS	<0.1	<0.1

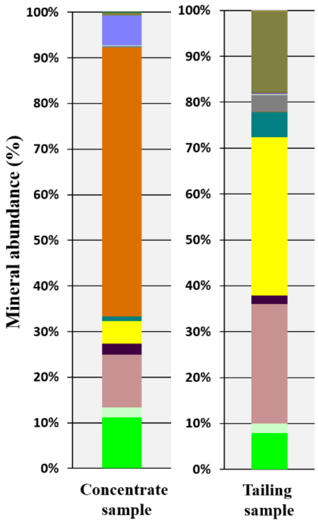

Fig. 7. Mineral abundance of concentrate and tailing samples

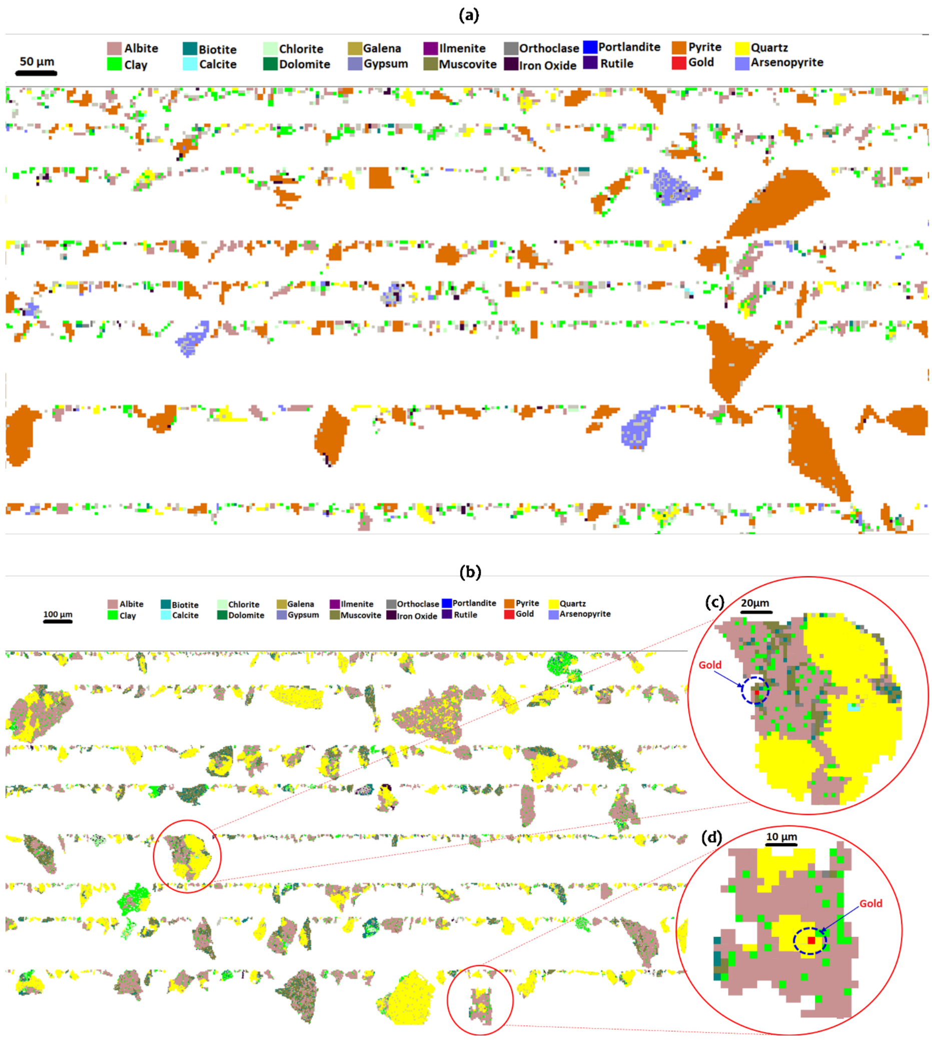

Fig. 8. Particle Mapping of (a) concentrate sample; (b) tailing sample; c) Grain of gold locked in albite mineral; d) Grain of gold locked in quartz

amount of arsenopyrite (Fig. 8.a). In addition, mineral mapping of tailing particles revealed that gold grains are enclosed in silicates such as albite (Fig. 8.c) and quartz (Fig. 8.d), with mesh sizes of less than 1µm. This demonstrates that the gold recovery yield achieved under the optimal flotation conditions is ultimate, as the gold is present as inclusions within the gangue, which is non-floatable.

The liberation data for the target minerals in both the concentrate and tailing samples are shown in Fig. 9. In the concentrate sample, pyrite grains are predominantly liberated (72%), with 25% in the middling fraction. These grains are primarily associated with clay minerals (26%) and iron oxides (18%) (Fig. 9.b), and enclosed in the same minerals with a percentage of 21% and 20% respectively (Fig. 9.c). On the other hand, arsenopyrite, is mainly found in the middling fraction (79%), with less than 5% liberated. The arsenopyrite grains are associated with pyrite (35%) and iron oxide (26%). For the gold grains, 20% are in the middling fraction, and associated with arsenopyrite (44%) and pyrite (11%) (Fig. 9.b). While 80% of gold grains are locked and mainly enclosed in arsenopyrite (11%) and pyrite (7%) (Fig. 9.c). In the tailings sample, most of the target minerals are locked, except for pyrite, which appears in the middling fraction (26%) (Fig. 9.d). Pyrite, arsenopyrite, and gold grains are all locked in quartz (30%-16%-22%), albite (3%-8%-14%), and clay minerals (27%-16%-11%). This further confirms the ultimate gold recovery by flotation, as gold and gold-bearing sulfides are predominantly encapsulated within these gangue minerals.

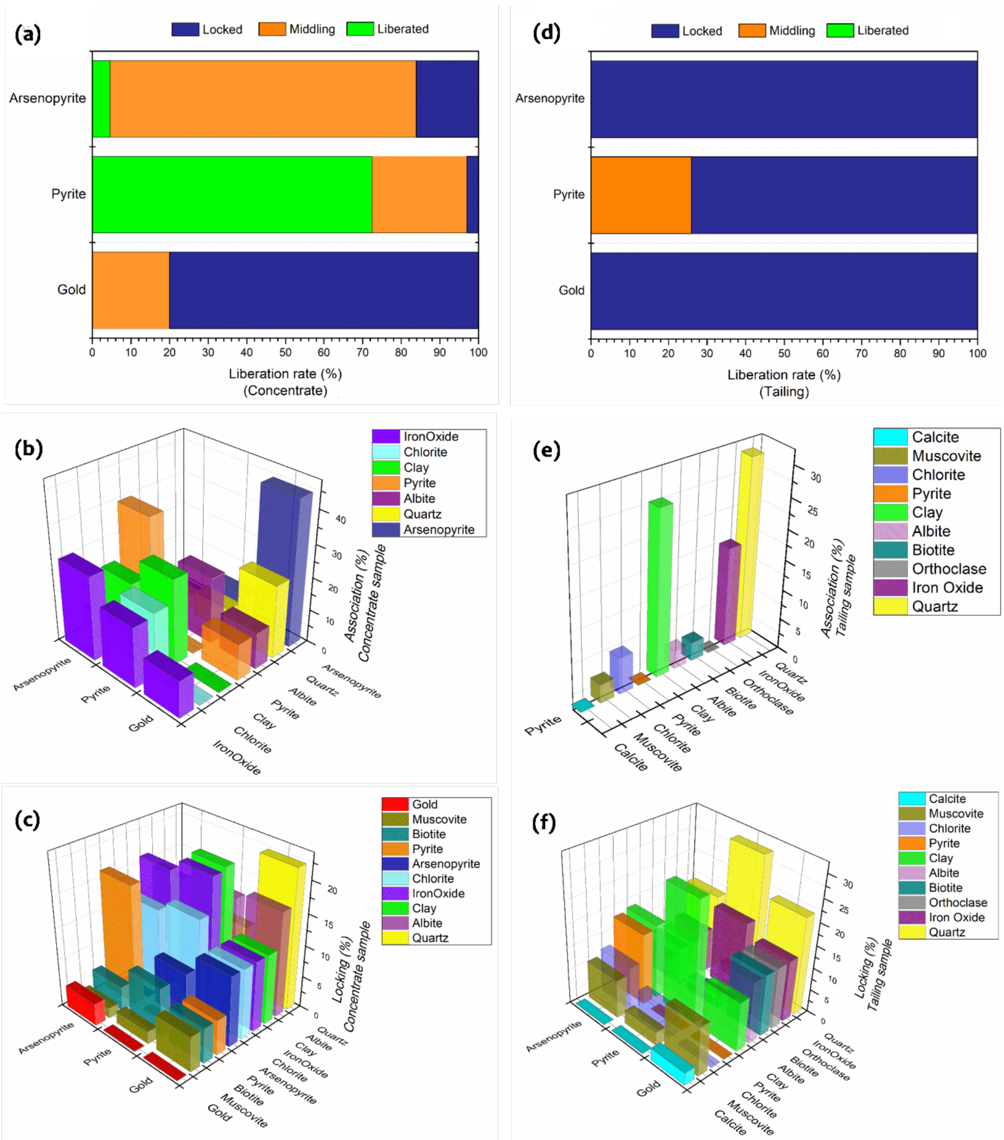

Fig. 9. Graphical analysis of the liberation, association, and locking characteristics of target minerals in concentrate and tailing samples. (a) Liberation rate; (b) association data and (c) locking data of target minerals in the concentrate sample. (d) liberation rate; (e) association data and (f) locking data of target minerals in the tailing sample

On the other hand, the significant improvement of gold recovery and gold grade achieved by increasing pH is likely due to the increased stability of the collector under alkaline conditions. To further investigate this behavior, FTIR spectroscopy was employed to analyze the functional groups and their corresponding vibration modes in the collector across the studied pH range (6-10) (Fig. **10**). The findings revealed that the main functional groups identified were consistent with those reported in previous studies (Amaral et al., 2021; Bai et al., 2018; Chandra et al., 2012; Eensalu et al., 2022; Juncal et al., 2015). The broad band at 3200–3600 cm^{-1} is attributed to the stretching modes of water molecules. The bands at 2800–2950 cm^{-1} and 1370–1470 cm^{-1} correspond to –CH stretching and bending modes. The transmission bands at 500–770 cm^{-1} and 1640 cm^{-1} are associated with –CO stretching modes. The band at 2090 cm^{-1} corresponds to the –CC bond, while the band at 990–1150 cm^{-1} is attributed to –CS stretching. Overall, it can be observed that all these bands weaken with decreasing pH, suggesting that the PAX collector degrades under low pH conditions, leading to a reduction in the flotation efficiency of gold and gold-bearing sulfides.

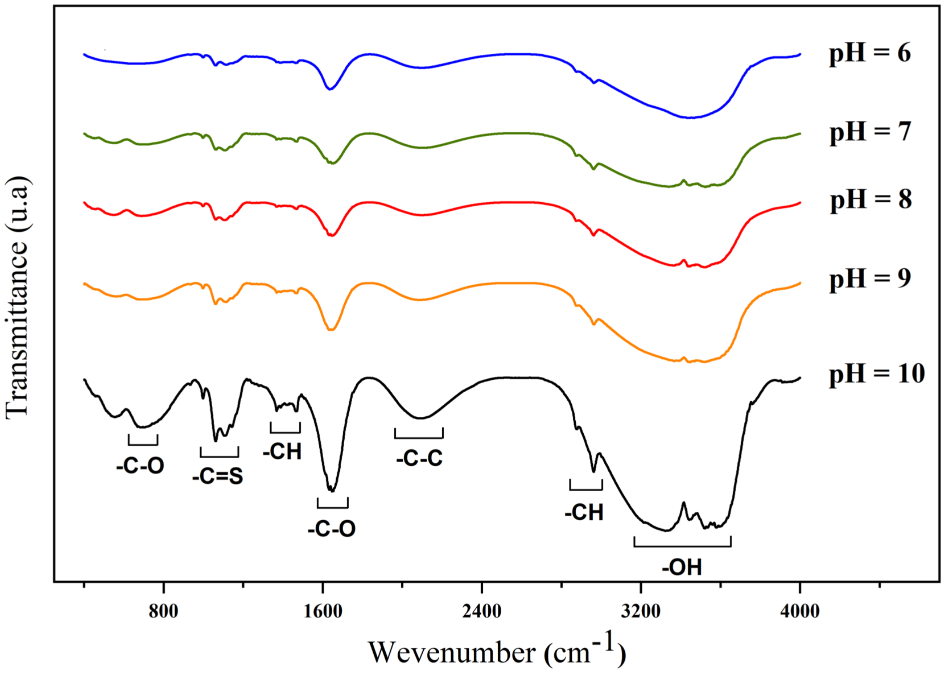

Fig. 10. FTIR spectra of PAX collector at different pH

4. Conclusions

This study examined the optimization of gold flotation in a refractory sulfidic gold ore using an integrated approach combining experimental design and automated quantitative mineralogy. A complete characterization of the ore using AQM and SEM revealed nanoscale gold inclusions (288.8 – 489.5 nm) within pyrite and arsenopyrite. Modal mineralogy indicated the sample predominantly comprises silicates (albite 36%, quartz 33.1%, and clay minerals 13.2%) and sulfides (pyrite 2.1% and arsenopyrite 0.3%). Using the Doehlert design, the optimal flotation conditions were identified as pH = 9.56 and D80 = 88 μm, achieving a gold recovery of 86.76% and a concentrate grade of 18.80 ppm from a feed grade of 2.61 ppm. Modal mineralogy and particle mapping confirmed effective separation, with sulfides dominating the concentrate (pyrite 58.9% and arsenopyrite 6.6%) and silicates dominating the tailings (quartz 34.6%, albite 26.2%, and muscovite 18%). Residual gold in the tailings was enclosed within non-floatable silicates, demonstrating ultimate recovery under these conditions. FTIR results linked improved flotation performance at higher pH to greater collector (PAX) stability. This approach highlights the effectiveness of integrating experimental design with advanced mineralogical tools for optimizing gold recovery in refractory ores.

Future work could validate the results at pilot or industrial scale, as the experiments were performed at laboratory scale, and scale-up effects in industrial flotation circuits, such as hydrodynamics and slurry heterogeneity, may affect the transferability of the optimized conditions.

Acknowledgments

The authors express their gratitude to the Reminex Research Center - Managem Group, for their support of this project.

References

ALLAN, G.C., WOODCOCK, J.T., 2001. *A review of the flotation of native gold and electrum*. Minerals Engineering, 14, 931–962.

AMARAL, C.N.R., OLIVEIRA, P.F., PEDRONI, L.G., MANSUR, C.R.E., 2021. *Viscoelastic behavior of hydrogel-based xanthan gum/aluminum lactate with potential applicability for conformance control*. Journal of Applied Polymer Science, 138.

BADRI, R., ZAMANKHAN, P., 2013. *Sulphidic refractory gold ore pre-treatment by selective and bulk flotation methods*. Advanced Powder Technology.

BAI, L., LIU, J., HAN, Y., JIANG, K., ZHAO, W., 2018. *Effects of xanthate on flotation kinetics of chalcopyrite and talc*. Minerals, 8.

BARBOUCHI, A., ER-RAQI, I., HAMCHI, M., IDOUHLI, R., KHADIRI, M., ABOUELFIDA, A., EL ALAOUI-CHRIFI, M.A., FAQIR, H., BENZAKOUR, I., BENZAKOUR, J., 2024a. *Chemical oxidation of arsenopyrite by strong oxidizing agents: For oxidative pretreatment of refractory arsenopyritic gold ores*. Acta Geodynamica et Geomaterialia, 185–194.

BARBOUCHI, A., ER-RAQI, I., IDOUHLI, R., KHADIRI, M.E., ABOUELFIDA, A., LOUARRAT, M., MIKALI, M., ALAOUI-CHRIFI, M.A. EL, FAQIR, H., BENZAKOUR, I., BENZAKOUR, J., 2024b. *Chemical oxidation of pyrite by strong oxidizing agents: For pretreatment of refractory pyritic gold ores.* Acta Montanistica Slovaca, 29, 773–786.

BARBOUCHI, A., LOUARRAT, M., MIKALI, M., BARFOUD, L., EL ALAOUI-CHRIFI, M.A., FAQIR, H., BENZAKOUR, I., IDOUHLI, R., KHADIRI, M. EDDINE, BENZAKOUR, J., 2024c. *Advancements in improving gold recovery from refractory gold ores/concentrates: A review*. Canadian Metallurgical Quarterly.

BARBOUCHI, A., AYADI, S., IDOUHLI, R., KHADIRI, M. EDDINE, ABOUELFIDA, A., BARFOUD, L., FAQIR, H., BENZAKOUR, I., BENZAKOUR, J., 2025a. *Highly efficient pretreatment for refractory gold ores using persulfate, catalyst and free radical based advanced oxidation processes to improve cyanidation*. Hydrometallurgy, 235.

BARBOUCHI, A., EL MOUDEN, A.A., LABBILTA, T., ANASSER, I., IDOUHLI, R., KHADIRI, M.E., ABOUELFIDA, A., FAQIR, H., BENZAKOUR, I., BENZAKOUR, J., 2025b. *Optimization of single-stage roasting process for pretreatment of refractory gold concentrate using experimental design*. Journal of Sustainable Metallurgy, 11, 2650–2662.

BROWN, S.D., TAULER, R., WALCZAK, B., 2009. *Comprehensive chemometrics: Chemical and biochemical data analysis*. Elsevier.

BU, X., XIE, G., PENG, Y., CHEN, Y., 2016. *Kinetic modeling and optimization of flotation process in a cyclonic microbubble flotation column using composite central design methodology*. International Journal of Mineral Processing, 157, 175–183.

CERQUEIRA, U.M.F.M., BEZERRA, M.A., FERREIRA, S.L.C., DE JESUS ARAÚJO, R., DA SILVA, B.N., NOVAES, C.G., 2021. *Doehlert design in the optimization of procedures aiming food analysis – A review*. Food Chemistry, 364.

CHANDRA, A.P., PUSKAR, L., SIMPSON, D.J., GERSON, A.R., 2012. *Copper and xanthate adsorption onto pyrite surfaces: Implications for mineral separation through flotation*. International Journal of Mineral Processing, 114–117, 16–26.

CHRYSSOULIS, S.L., DIMOV, S.S., 2004. *Optimized conditions for selective gold flotation by ToF-SIMS and ToF-LIMS*. Applied Surface Science.

DUNNE, R., 2016. *Flotation of gold and gold-bearing ores*. Gold Ore Processing: Project Development and Operations.

EENSALU, J.S., TÕNSUAADU, K., ADAMSON, J., OJA ACIK, I., KRUNKS, M., 2022. *Thermal decomposition of tris(O-ethyldithiocarbonato)-antimony(III)—a single-source precursor for antimony sulfide thin films*. Journal of Thermal Analysis and Calorimetry, 147, 4899–4913.

EL MAGUANA, Y., ELHADIRI, N., BOUCHDOUG, M., BENCHANAA, M., BOUSSETTA, A., 2018. *Optimization of preparation conditions of novel adsorbent from sugar scum using response surface methodology for removal of methylene blue*. Journal of Chemistry, 2018.

FENG, Q., ZHANG, Y., ZHANG, G., HAN, G., ZHAO, W., 2025. *Innovative scheme for hemimorphite flotation: Synergistic activation performance and mechanism*. International Journal of Minerals, Metallurgy and Materials, 32, 1297–1308.

GAO, J., BU, X., ZHOU, S., WANG, X., ALHESHIBRI, M., PENG, Y., XIE, G., 2022. *Graphite flotation by β-cyclodextrin/kerosene Pickering emulsion as a novel collector*. Minerals Engineering, 178.

HAMMERSCHMIDT, J., GÜNTNER, J., KERSTIENS, B., CHARITOS, A., 2016. *Roasting of gold ore in the circulating fluidized-bed technology*. Gold Ore Processing: Project Development and Operations.

JIA, Y., TAN, Q., SUN, H., ZHANG, Y., GAO, H., RUAN, R., 2019. *Sulfide mineral dissolution microbes: Community structure and function in industrial bioleaching heaps*. Green Energy and Environment.

JUNCAL, L.C., COZZARÍN, M.V., ROMANO, R.M., 2015. *Conformational and spectroscopic study of xanthogen ethyl formates*. Spectrochimica Acta Part A: Molecular and Biomolecular Spectroscopy, 139, 346–355.

LUNT, D., WEEKS, T., 2016. *Process flowsheet selection*. Gold Ore Processing: Project Development and Operations.

MESA ESPITIA, S.L., LAPIDUS, G.T., 2015. *Pretreatment of a refractory arsenopyritic gold ore using hydroxyl ion*. Hydrometallurgy, 153, 106–113.

MIKALI, M., BARBOUCHI, A., IDOUHLI, R., ABOUELFIDA, A., YAACOUBI, A., BENZAKOUR, I., FAQIR, H., BOULAAMAIL, A., BACAOUI, A., 2023. *Electrochemical behavior of silver during cyanidation in the presence of sulfide minerals*. Chemical Papers, 77(4), 2103–2113.

MILLER, P., BROWN, A.R.G., 2016. *Bacterial oxidation of refractory gold concentrates*. Gold Ore Processing: Project Development and Operations.

MOSLEMI, H., GHARABAGHI, M., 2017. *A review on electrochemical behavior of pyrite in the froth flotation process*. Journal of Industrial and Engineering Chemistry.

REN, X., BU, X., TONG, Z., DONG, L., MA, Z., WANG, J., CAO, M., QIU, S., 2024. *Influences of plasma treatment parameters on the hydrophobicity of cathode and anode materials from spent lithium-ion batteries*. Waste Management, 184, 120–131.

RODRÍGUEZ-RODRÍGUEZ, C., NAVA-ALONSO, F., URIBE-SALAS, A., 2018. *Arsenopyrite oxidation with ozone: Stoichiometry and kinetics*. Ozone Science & Engineering, 40, 284–292.

ROGOZHNIKOV, D., KARIMOV, K., SHOPPERT, A., DIZER, O., NABOICHENKO, S., 2021. *Kinetics and mechanism of arsenopyrite leaching in nitric acid solutions*. Hydrometallurgy, 199.

TANG, Y., YANG, W., CHEN, S., SHEN, Z., FENG, Q., ZHANG, Q., 2026. *A green and biodegradable depressant for efficient flotation separation of smithsonite from calcite*. Separation and Purification Technology, 380.

THOMAS, K.G., PEARSON, M.S., 2016. *Pressure oxidation overview*. Gold Ore Processing: Project Development and Operations.

XUE, Y., WU, P., LÜ, Y., SHAN, H., XU, X., YU, B., CHEN, X., ZHANG, X., XIONG, C., 2026. *Cavitation-flotation coupling purification of natural flake graphite*. Separation and Purification Technology, 382.

YANG, W., TANG, Y., HUANG, B., HAN, G., FENG, Q., 2025. *Enhanced flotation of sulfidized smithsonite in a Cu–Pb dual activation system*. Green and Smart Mining Engineering, 2, 8–17.

ZHOU, J., GU, Y., 2016. *Geometallurgical characterization and automated mineralogy of gold ores*. Gold Ore Processing: Project Development and Operations, 95–111.

ZHOU, S., TONG, Z., DONG, L., BU, X., NI, C., XIE, G., ALHESHIBRI, M., 2023. *Influence of single and combined ultrasounds assisted flake graphite flotation*. Ultrasonics Sonochemistry, 99.